Distinct functional roles for hopanoid composition in the chemical tolerance of *Zymomonas mobilis*

Running title: Hopanoids in bacterial ethanol tolerance

Léa Brenac[1†], Edward E.K. Baidoo[1], Jay D. Keasling[1,2,3-8], and Itay Budin[1,2,9*]

[1.] Joint BioEnergy Institute, 5885 Hollis Street, Emeryville, CA 94608

[2.] Department of Chemical & Biomolecular Engineering, University of California, Berkeley, Berkeley CA 94720

[3.] Department of Chemistry, University of California, Berkeley, Berkeley, CA 94720

[4.] Department of Bioengineering, University of California, Berkeley, Berkeley CA 94720

[5.] QB3 Institute, University of California, Berkeley, Berkeley, CA 94270

[6.] Biological Systems & Engineering, Lawrence Berkeley National Laboratory, Berkeley, CA 94720

[7.] The Novo Nordisk Foundation Center for Sustainability, Technical University of Denmark, Denmark

[8.] Center for Synthetic Biochemistry, Institute for Synthetic Biology, Shenzhen Institutes for Advanced Technologies, Shenzhen, CN

[9.] Department of Chemistry & Biochemistry, University of California, San Diego, La Jolla, CA 92093

[†.] Current affiliation: Lonza Ltd, Visp Switzerland

*Correspondence: ibudin@ucsd.edu

Summary:

Hopanoids are abundant membrane lipids found in diverse bacterial lineages, but their physiological roles are not well understood. The ethanol fermenter *Zymomonas mobilis* features the highest measured concentration of hopanoids, leading to the hypothesis that these lipids can protect against bacterial solvent toxicity. However, the lack of genetic tools for manipulating hopanoid composition *in vivo* has limited their further functional analysis. Because of polyploidy (> 50 genome copies per cell), we found that disruptions of essential hopanoid biosynthesis (*hpn*) genes in *Z. mobilis* act as genetic knockdowns, reliably modulating the abundance of different hopanoid species. Using a set of *hpn* transposon mutants, we demonstrate that both reduced hopanoid content and modified hopanoid head group composition mediate growth and survival in ethanol. In contrast, the amount of hopanoids, but not their polar group composition, contributes to fitness at low pH. Spectroscopic analysis of model membranes showed that hopanoids protect against several ethanol-driven phase transitions in membrane structure, including lipid interdigitation and bilayer dissolution. We propose that hopanoids act through a combination of hydrophobic and inter-lipid hydrogen bonding interactions to stabilize bacterial membranes against solvent stress.

Keywords:

Lipids, ethanol, fermentation, membrane structure

53 **Introduction:**
54
55 Triterpenoids are a class of cyclized lipids used by cells as bulk membrane building
56 blocks. The canonical triterpernoids are eukaryotic sterols, in which squalene is oxidized
57 before cyclization, leaving a hydroxyl to act as a polar head group. With very few
58 exceptions (Pearson, Budin, & Brocks, 2003), bacteria instead synthesize hopanoids, in
59 which squalene is first cyclized into hopene and then derivatized with polar groups
60 (Ourisson & Rohmer, 1992). Hopanoids are thought to mimic the well-known effects of
61 sterols on membrane ordering and permeability (Kannenberg, Blume, McElhaney, &
62 Poralla, 1983; Poger & Mark, 2013; Saenz, Sezgin, Schwille, & Simons, 2012). Unlike
63 sterols, however, they are generally present in complex mixtures of several derivatives,
64 which could diversify their functions. They are also not as widespread, being absent in a
65 majority of cultured bacterial strains (Rohmer, Bouvier-Nave, & Ourisson, 1984) and
66 environmental samples (Pearson, Flood Page, Jorgenson, Fischer, & Higgins, 2007).
67
68 In bacteria with non-essential hopanoids, hopanoid biosynthesis (*hpn*) mutants have been
69 used to identify functional roles related to chemical stress. In *Burkholderia cenocepacia*,
70 hopanoid-free cells were found to be sensitive to low pH and detergents (Schmerk,
71 Bernards, & Valvano, 2011), while in *Rhodopseudomonas palustris* they are more
72 sensitive to both low and high pH (Welander et al., 2009) as well as bile salts (Welander
73 et al., 2012). In *Bradyrhizobium diazoefficiens*, mutants lacking elongated hopanoids
74 showed membrane defects and were sensitive to antibiotics, acid, and detergent (Kulkarni
75 et al., 2015). The biophysical basis for these phenotypes has not been well studied, nor
76 have physiological roles been characterized in bacteria where hopanoids are essential.
77
78 Because of its unusual glycolytic metabolism (Flamholz, Noor, Bar-Even, Liebermeister,
79 & Milo, 2013), the alphaproteobacterium *Z. mobilis* produces ethanol approaching
80 theoretical yields (Sprenger, 1996), leading to its adoption for industrial fermentation
81 applications (Ming He et al., 2014). Native to palm wine fermenters (Swings & De Ley,
82 1977), *Z. mobilis* features a remarkable tolerance to ethanol, with reported growth in
83 media containing up to 16% (v/v) ethanol (Lee, Skotnicki, Tribe, & Rogers, 1980). It also
84 features a high abundance of hopanoids in its inner membrane – up to 50% of all lipids in

the cell (Hermans, Neuss, & Sahm, 1991) – suggesting that these lipids could be important for its ability to withstand ethanol.

Like other solvents, ethanol alters the lipid packing (Vierl, Löbbecke, Nagel, & Cevc, 1994) and phase properties (Gurtovenko & Anwar, 2009) of model membranes. In principle, the condensing effect of hopanoids, analogous to eukaryotic sterols (Perzl et al., 1998; Saenz et al., 2012), could buffer against changes to membrane structure induced by solvents. However, in contrast to longer chain alcohols that fluidize membranes, the physicochemical effects of ethanol are complex, and include the induction of membrane phase transitions that increase membrane ordering (Vierl et al., 1994). Notably, in other ethanol-tolerant microbial fermentors (budding yeast), unsaturated fatty acids have been shown to mediate ethanol tolerance (Thomas, Hossack, & Rose, 1978; You, Rosenfield, & Knipple, 2003) and these lipids are thought to have opposing biophysical effects as hopanoids and other triterpenoids. In *Z. mobilis*, early lipid analyses using thin layer chromatography reported an increase in hopanoids during ethanol exposure (Bringer, Thomas, Poralla, & Sahm, 1985), but later work using modern mass spectrometry tools and transcriptomics showed no link between ethanol and hopanoid biosynthesis (Hermans et al., 1991; Moreau, Powell, Fett, & Whitaker, 1997) or *hpn* expression (Ming-xiong He et al., 2012), respectively. Therefore, it is still not established whether hopanoids contribute to the ethanol tolerance of *Z. mobilis*.

Testing physiological functions for hopanoid composition requires genetic tools to modulate their abundance and stoichiometry in cells. In *Z. mobilis,* a transposon-based gene disruption has previously been used to generate loss of function mutants to carry out systematic fitness analyses (Skerker et al., 2013). Surprisingly, this effort yielded transposon insertions in essential genes, e.g. those encoding for RNA/DNA polymerases. Such an effect was proposed to result from polyploid cells containing both mutant alleles, carrying antibiotic resistance markers, and functional ones, carrying essential genes. We hypothesized that this dynamic could reduce the copy number of biosynthetic genes, thereby functioning as genetic knockdowns and allowing for functional studies of hopanoid composition.

116

117 **Results:**

118

119 We first collected a redundant set of 25 Tn5 mutants of the *Z. mobilis* strain ZM4 covering
120 annotated genes in the hopanoid biosynthesis pathway (Fig. 1A). Mutants with
121 transposons at different positions in the same genes showed identical fitness profiles (Fig.
122 S1), indicating that insertions acted as null alleles. When grown under antibiotic selection
123 for the transposon, PCR analysis of transposon-inserted *hpn* genes showed the existence
124 of both wild-type and mutated alleles (Fig. 1B), with varying apparent abundances. To
125 confirm that heterozygosity was due to polyploidy, we measured chromosome numbers
126 per cell directly using a qPCR-based approach (Fig. 1C). We found that *Z. mobilis* cells
127 were highly polyploid, containing > 50 copies of two different genomic loci under our
128 growth conditions. In contrast, a monoploid bacterium (*E. coli* in minimal medium)
129 featured 1-2 genome copies per cell by this method. We quantified the transposon
130 insertion rate for *hpn* mutants using high coverage genome sequencing, quantifying the
131 number of reads matching to each allele (Fig 1D). The mutant allele frequency ranged
132 from 31 to 100%, with non-duplicated genes early in the pathway featuring the lowest
133 abundance and non-essential genes late in the pathway mimicking full knockouts (Table
134 S1).

135

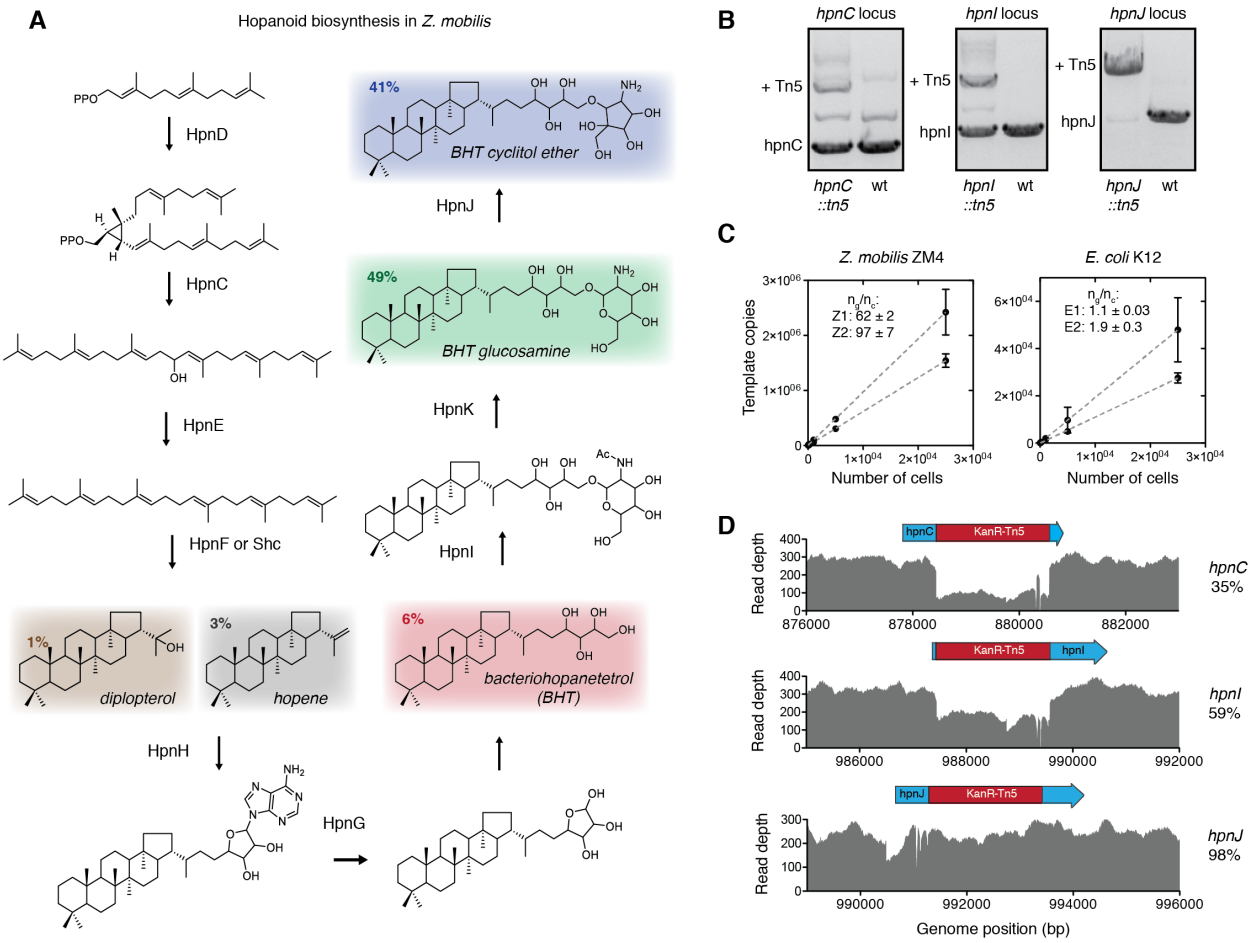

Fig. 1: Genetic characterization of *hpn* transposon mutants in *Z. mobilis*. (**A**) Hopanoid biosynthesis in *Z. mobilis* occurs via a multistep pathway catalyzed by products of highly conserved *hpn* genes. Colored species indicate mature products and their reported (Hermans et al., 1991) abundance in wild type cells (as a % of total hopanoid weight content). (**B**) Characteristic colony PCRs showing the *hpn*::Tn5 strains contain both native *hpn* alleles and mutant *hpn*::Tn5 ones in varying amounts. In mutants early in the pathway (e.g. *hpnC*), the native allele is dominant over the mutant, but this is reversed for those late in the pathway (e.g. *hpnJ*). (**C**) Measurement of ploidy in *Z. mobilis* using qPCR of DNA extracted from counted cells, whose amplification was normalized with that of purified template standards. For *Z. mobilis* (left), this analysis yielded high genome copy numbers (60-100) for two different loci (Z1 and Z2). In contrast, *E. coli* grown in minimal media, where it is monoploid, showed a low copy number (1-2, E1 and E2) by the same method (right). Values represent mean +/- SEM, n=3. (**D**) Quantification of mutant allele abundance by deep sequencing of genomic DNA. Reads for each mutant were mapped to the genome sequence containing the transposon, and read coverage in the transposon was used to quantify the fraction of genome copies carrying the mutant allele. Shown are three examples that correspond to colony PCRs in panel (**B**); for each, a gene map with the transposon insertion is shown above the coverage plot. Quantification for the rest of the mutants is found in Table S1.

157

158 Since *hpn* mutants reduce the fraction of functional alleles in a cell, we hypothesized that
159 they would reduce the abundance of the downstream product of each Hpn enzyme. To
160 test this, we used a combination of mass spectrometry approaches to characterize the
161 hopanoid composition of mutants grown under transposon selection. The products of
162 squalene cyclization, hopene (Fig. 2A) and diplopterol (Fig. 2B), were measured by gas
163 chromatography coupled to mass spectrometry (GC-MS) of silylated lipid extracts (Fig.
164 S2A). Both showed decreased abundance in squalene synthase (*hpnC*, *hpnD*) mutants,
165 consistent with their position upstream in the pathway. Lipids from *hpnF* and *shc* mutants,
166 which exhibited almost complete disruption, showed distinct distributions of squalene
167 cyclization products: the *shc* mutant accumulated less hopene, while the *hpnF* mutant
168 accumulated less diplopterol. This difference suggests differing product preferences
169 these SHCs. Lipids from the *hpnH* mutant exhibited higher hopene levels, consistent with
170 the role of HpnH in converting hopene to adenosylhopane. Later genes in the pathway
171 (*hpnG, hpnI*, *hpnK, hpnJ)* mildly altered levels of these products, possibly reflecting
172 feedback regulation in the pathway, as have been well-characterized for sterol
173 biosynthesis (Espenshade & Hughes, 2007).

174

175

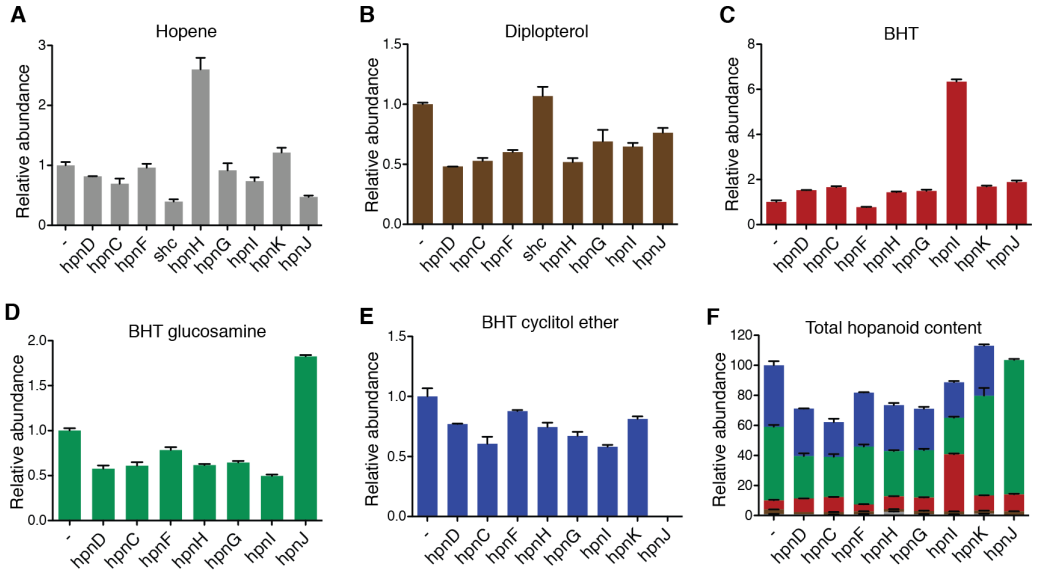

176
177

178 **Fig. 2**: Composition of mature hopanoid species in *hpn* mutants or control cells (-). Cells
179 were grown in RM media for 20-22 hours under kanamycin selection for the transposon

180 and lipids were extracted as described in the Methods. Each species is color coded by
181 their structures in Fig. 1a, and values are normalized to control cells. The abundance of
182 hopene (**A**) and diplopterol (**B**) were measured by GC-MS of silylated lipid extracts, while
183 BHT (**C**), BHT glucosamine (**D**) and BHT cyclitol ether (**E**) were measured by LC-APCI-
184 TOF-MS of acetylated lipid extracts. Total hopanoids (**F**) are normalized by the absolute
185 abundance of each species in wild type background as previously measured (Hermans
186 et al., 1991). Error bars indicate mean +/- SD, n = 3 independent cultures.
187

188 We next analyzed the distribution of elongated hopanoids, which compose the majority
189 of final hopanoid products in *Z. mobilis*, using liquid chromatography coupled to
190 atmospheric pressure chemical ionization time of flight mass spectrometry (LC-APCI-
191 TOF-MS) (Fig. 2C-E, Fig. S2B-C). Mutants targeting enzymes upstream of the elongated
192 hopanoids all showed reduced abundance of all these products, but did not alter their
193 stoichiometry. Instead, it was mutants of the three genes downstream of
194 bacteriohopanetetrol (BHT) in the pathway (*hpnI*, *hpnK* and *hpnJ*) that altered elongated
195 hopanoid distribution. The *hpnI* mutant exhibited an accumulation of BHT accompanied
196 by a reduction of the BHT derivatives. Analyses of the *hpnK* mutant was hindered by the
197 acetylation of BHT glucosamine during lipid derivatization. However, the increased ratio
198 of BHT glucosamine to BHT cyclitol ether (2:1) we observed was consistent with its
199 expected role as a deacetylase. In the *hpnJ* mutant, no BHT cyclitol ether could be
200 detected, in agreement with it being near complete gene knock out (98% mutant alleles).
201

202 Lipid analysis confirmed the proposed biosynthetic route for hopanoids in *Z. mobilis* and
203 showed that transposon disruptions act as functional knockdowns, resulting in changes
204 in hopanoid abundance and distribution (Fig. 2F). We tested whether these changes
205 modulate the physical properties of lipid bilayers using the anisotropy-based probe di-
206 phenyl-hexatriene (DPH), a classic test of ordering in the hydrophobic membrane core
207 (Suurkuusk, Lentz, Barenholz, Biltonen, & Thompson, 1976). Membranes prepared from
208 extracted lipids with reduced hopanoid content showed significantly lower DPH anisotropy
209 (Fig. 3), while those with altered head group composition showed a milder effect. This
210 pattern is consistent with the hopene moiety – common to all hopanoids – being
211 responsible for increasing hydrocarbon packing in the membrane, similar to the effect of

212 sterols. All *Z. mobilis* compositions featured a higher anisotropy compared to membranes
213 assembled from lipids extracted from *E. coli* MG1655, which lack hopanoids.
214

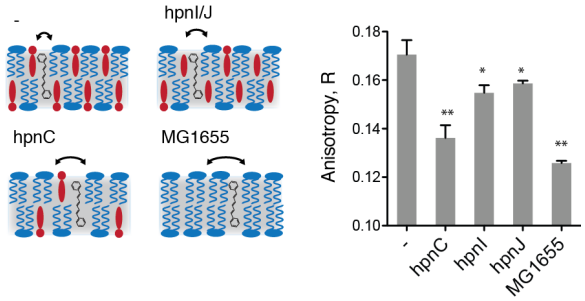

215
216
217 **Fig. 3:** The dependence of bilayer order, as measured by DPH anisotropy, on hopanoid
218 composition in liposomes. Liposomes were prepared using lipids extracted from early-
219 stationary phase cultures for each *hpn* mutant, cells with intact hopanoids (-), or
220 hopanoid-free *E. coli* (MG1655). Steady-state anisotropy of DPH incubated with the
221 liposomes was measured as a unit-less ratio $R = (I_A - I_B) / (I_A + 2\ I_B)$, where I_A and I_B are
222 the emission (430 nm) intensities parallel and perpendicular, respectively, to the
223 polarization of the excitation (360 nm). Cartoons on the left diagram the compositional
224 differences for each sample, as well as the relative motion of the probe within the bilayer's
225 hydrophobic core. In the diagrams, the blue and red species are phospholipids and
226 hopanoids, respectively. Error bars indicate mean +/- SEM (n=3). Unpaired t-tests
227 compare indicated lipid composition against the control (-): *, $p < 0.05$; **, $p < 0.01$.
228

229 We sought to use *hpn* mutants to assess the proposed physiological role for hopanoid
230 composition in *Z. mobilis* ethanol tolerance. In standard rich media (RM), exponential
231 growth rates of different mutants were correlated to their total hopanoid content, likely
232 reflecting physiological roles for these lipids under non-stressed conditions (Fig. S3). We
233 focused further investigation on a set of strains that sampled different aspects of hopanoid
234 composition: reduced total hopanoid content (*hpnC* or *hpnD*), reduced accumulation of
235 elongated hopanoids (*hpnI*), or absence of BHT cyclitol ether (hpnJ), comparing each
236 with the behavior of a kanamycin-resistant control (Fig. 4A). For growth with 8% (v/v)
237 ethanol, *hpn* mutants showed a significantly larger growth defect compared to the control
238 (Fig. 4A-B). This effect was significant both for mutants with reduced hopanoid content
239 and those with altered elongated hopanoids. A similar pattern was found for toxicity,
240 measured by colony forming units, after acute (30 min) exposure to high ethanol
241 concentration (20%), with each mutant featuring significantly reduced survival (Fig. 4C).

242 Both hopanoid abundance and stoichiometry are thus functional for *Z. mobilis* ethanol
243 fitness.
244

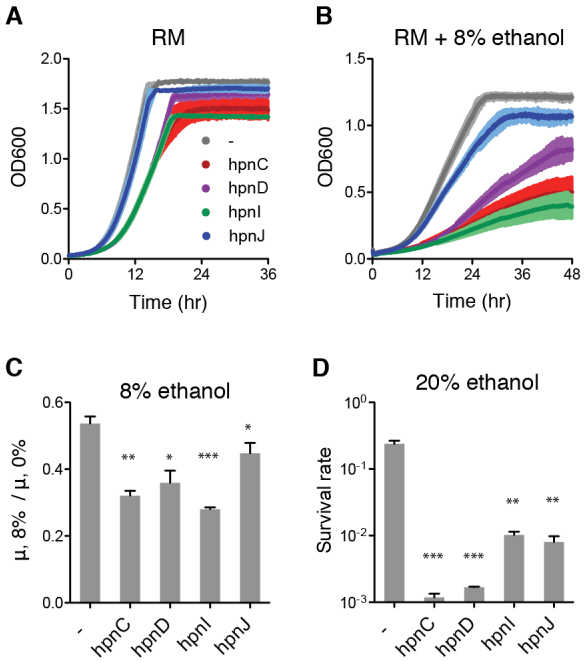

245
246
247
248 **Fig. 4:** The effect of hopanoid knockdowns on *Z. mobilis* ethanol tolerance. A subset of
249 *hpn* mutants sampling hopanoid composition were chosen for analysis. (**A**) Under
250 standard conditions on rich medium (RM), *hpn* mutants grow similarly to control cells (-),
251 which feature a kanamycin cassette in non-essential lysine exporter. In 8% v/v ethanol,
252 however, *hpn* mutants show visible growth defects compared to control cells. (**B**) The
253 relative growth rates in 8% vs. 0% ethanol (μ, 8% / μ, 0%) are significantly reduced for all
254 *hpn* mutants compared to the control. (**C**) The *hpn* mutants also show significant
255 increases in acute toxicity to ethanol, as measured by their survival rate after 30 min in
256 20% v/v ethanol. Error bars indicate mean +/- SEM, n = 3 independent cultures. Unpaired
257 t-tests were used to assess significance against control cells (-): *, $p < 0.05$; **, $p < 0.01$;
258 ***, $p < 0.001$.
259

260 In addition to ethanol, we considered other forms of chemical stress tolerance that would
261 be characteristic of the native environment for *Z. mobilis*. Fermentation is characterized
262 by acidic conditions, and *Z. mobilis* grows robustly between pH 3 and 4, matching the
263 acidity of palm wine (Swings & De Ley, 1977). As discussed above, hopanoids have been
264 known to increase ethanol tolerance in other bacteria in which they are not essential.
265 Accordingly, we found that *hpn* mutants with reduced total hopanoid content (*hpnC* and
266 *hpnD*) showed reduced growth rates at pH 3.9 (Fig. 5A) and survival at pH 2.5 (Fig. 5B).

However, mutants that altered hopanoid composition, but not total abundance (*hpnI* and *hpnJ*), showed no significant change in acid tolerance. The presence of hopanoids is likely essential for *Z. mobilis* to thrive in acidic conditions, but the stoichiometry of head group species is less important as compared to that for ethanol toxicity.

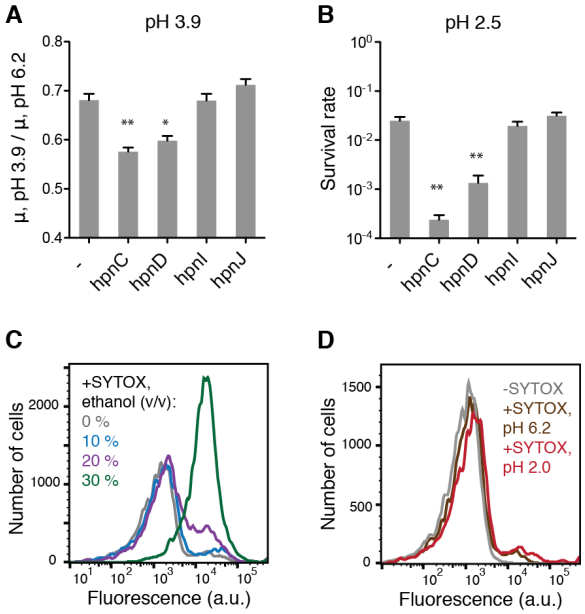

Fig. 5: In contrast to ethanol, acid tolerance is dependent on hopanoid abundance, but not head group composition. (**A**) Mutants (*hpnC* and *hpnD*) with reduced hopanoid abundance show impairment in growth at pH 3.9 vs. pH 6.2, while those that affected hopanoid composition (*hpnI* and *hpnJ*) do not. (**B**) A similar pattern was observed for acute toxicity at high acidity (30 min at pH 2.5), as measured by colony forming units. Error bars indicate mean +/- SEM, n = 3 independent cultures. Unpaired t-tests were used to assess significance against control cells (-): *, $p < 0.05$; **, $p < 0.01$; ***, $p < 0.001$. (**C**) SYTOX staining of wild-type *Z. mobilis* cells with increasing ethanol concentrations shows that cell death between 20 and 30% (v/v) ethanol corresponds to a loss of membrane integrity. When permeabilization occurs, the polar dye can bind to cellular nucleic acids, leading to increased fluorescence. (**D**) In contrast, staining of cells in extreme acidity (pH 2.0) did not exhibit a loss in membrane integrity. Cells under these conditions showed no survival in physiological tests, suggesting that a loss of membrane structure is the cause of ethanol but not acid toxicity.

The discrepancy the role of hopanoid stoichiometry in acid vs. ethanol could reflect different modes of lethality imposed by these chemical stresses. We hypothesized that

293 while solvent exposure (e.g. ethanol) would lead to a loss of membrane structure, acid
294 toxicity would occur by a different mechanism – such passive permeability of protons
295 leading to cytoplasmic acidification – that is not dependent on loss of membrane integrity.
296 To test this difference, we assayed membrane integrity using SYTOX staining. Cells
297 incubated with ethanol exposure showed an increase membrane permeability at 20 and
298 30% v/v ethanol, corresponding to the toxicity threshold (Fig. 5C). However, those
299 exposed to lethal acidic conditions (pH 2.0) did not show increased staining (Fig. 5D),
300 indicating that acid does not lead to a loss in membrane integrity as ethanol exposure
301 does.
302
303 To further explore the mechanisms by which hopanoids protect membranes against
304 ethanol-mediated permeabilization, we carried out spectroscopic assays using liposomes
305 assembled from *hpn* mutant lipid extracts. Because of its hydrophilicity, ethanol interacts
306 with lipid membranes at the solvent-bilayer interface (Holte & Gawrisch, 1997). We
307 therefore employed the fluorescent probe Laurdan, whose emission is sensitive to solvent
308 access near the head group interface (Parasassi, Krasnowska, Bagatolli, & Gratton,
309 1998), to track changes to membrane structure in response to ethanol. As bilayers
310 become disordered, they allow in more polar solvents, and Laurdan emission becomes
311 red-shifted. This emission shift is quantified with a General Polarization (GP) ratio.
312 Because Laurdan remains partitioned in lipid membranes independent of ethanol
313 concentration (Zeng & Chong, 1995), changes in GP reflect changes in membrane
314 ordering.

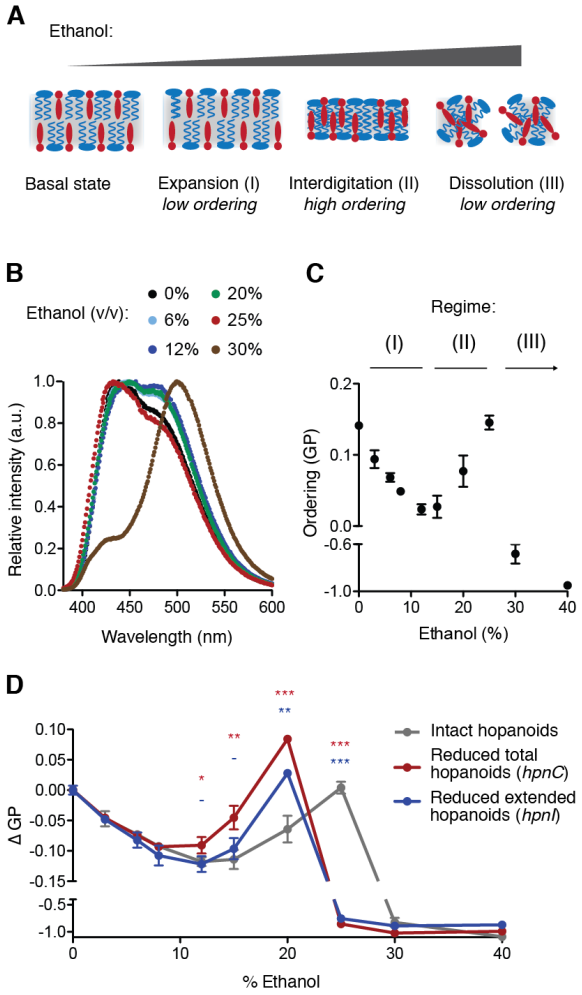

Fig. 6: The hopanoid composition of *Z. mobilis*-derived liposomes mediates changes to bilayer structure induced by ethanol. (**A**) Cartoon showing the sequential phase transitions in membranes caused by increasing ethanol concentrations, including bilayer expansion (I), lipid interdigitation (II), and membrane dissolution (III). The blue and red species representing phospholipids and hopanoids, respectively. (**B**) Emission spectra of Laurdan in liposomes reconstituted from extracted *Z. mobilis* lipids with different amounts of ethanol. At low concentrations (0-10% v/v), ethanol red-shifts Laurdan emission, indicating more solvent access to the bilayer. At intermediate concentrations (10-25%), this effect is reversed due to an ordered membrane phase with interdigitated lipids. At high concentrations (> 30%), emission is strongly red-shifted, indicating solubilization of the membrane. (**C**) Quantification of membrane ordering, measured as Laurdan GP, and its triphasic dependence on ethanol concentration in membranes containing *Z. mobilis* lipids. Each of the three regimes (I, II, III) corresponds to a structural transition diagrammed in panel a. (**D**) The effect of mutant lipid compositions with hopanoid content (*hpnC*) or changes in its head group composition (*hpnI*) on changes to Laurdan GP with increasing ethanol concentrations. Mutant liposomes show a stronger increase in GP in moderate ethanol concentrations (12-20%), indicating a more pronounced interdigitated

phase, as well as a reduced threshold for bilayer dissolution at high ethanol concentration. Error bars indicate mean +/- SD, n = 3 independent liposome preparations. Unpaired t-tests were used to assess significance against liposomes with intact hopanoids: *, $p < 0.05$; **, $p < 0.01$; ***, $p < 0.001$.

We found that Laurdan GP had a triphasic dependence on ethanol concentration, which track previously identified membrane structural changes (Fig. 6A-C). Initially, ethanol acts to disorder membranes, increasing head group spacing (bilayer expansion) and solvent accessibility, thereby reducing GP (regime I). At a critical concentration (~10%), the trend is reversed as phospholipid acyl chains become interdigitated across the bilayer, a gel-like phase transition (Mou, Yang, Shao, & Huang, 1994; Simon & McIntosh, 1984) that increases GP (regime II). At a second critical concentration (>25%), Laurdan emission strongly red shifts, reflecting the dissolution of the bilayer structure at high ethanol concentrations that correspond to lethality in cells (regime III). The three regimes of the ethanol concentration vs. Laurdan GP relationship can thus be used to interrogate the specific structural effects on lipid membranes.

Consistent with our physiological data, hopanoid composition mediated the changes to membrane structure induced by ethanol (Fig. 6D). We compared the changes to Laurdan GP in liposomes made from extracts with mutants with reductions in total (*hpnC*) and extended (*hpnI*) hopanoids. Under basal conditions (0% ethanol), reductions in total (*hpnC*) and extended (*hpnI*) hopanoids led to decreased membrane ordering, with the latter having the larger effect (Fig. S4). This is in contrast with membrane ordering of the hydrophobic core measured with DPH (Fig. 3), likely reflecting the importance of the hopanoid polar head group in driving ordering at the solvent-bilayer interface, which Laurdan is sensitive to. This trend continued during bilayer expansion at 8% ethanol, which led to uniform decrease in Laurdan GP among all compositions. However, at higher ethanol concentrations (20%), ordering was significantly higher in hopanoid-depleted (*hpnC*) membranes, indicating a more pronounced interdigitated phase compared to membranes with wild type levels of hopanoids. At 25% ethanol, both *hpnC* and *hpnI* liposomes showed a dramatic drop in Laurdan GP, indicating a loss of membrane structure while control liposomes remained intact. Therefore, both hopanoid abundance

367 and head group composition act to prevent membrane dissolution at high ethanol
368 concentrations.
369
370 **Discussion:**
371
372 Although widespread among bacteria, hopanoids remain a poorly understood class of
373 membrane lipids. To better understand their function, we sought a genetic system for
374 modulating the composition hopanoids in *Z. mobilis*, a bacterium in which these lipids are
375 both highly abundance and essential for growth. Because of its high polyploidy, we found
376 that transposon mutants of essential *hpn* genes – when grown under selection – act as
377 specific knockdowns of several steps in hopanoid biosynthesis. Using a set of *hpn*
378 mutants, we characterized the effects of changes in hopanoid abundance and
379 composition on the *Z. mobilis* physiology and the biophysical properties cell-derived
380 membranes. Notably, we established that both the abundance of hopanoids and their
381 polar head groups play key roles in dictating ethanol tolerance. A role for hopanoids in
382 the ability of *Z. mobilis* to grow and survive in high ethanol concentrations has been
383 hypothesized, but had been previously difficult to test. Because of the importance of this
384 bacterium to industrial ethanol production, we expect that further engineering of hopanoid
385 biosynthesis could be an avenue to tune its fermentation capabilities or to increase
386 solvent tolerance in other, less-robust hosts.
387
388 We contrasted the role of hopanoids in ethanol tolerance with that of another chemical
389 stress, acid. Unlike for ethanol, the ability for hopanoids to impart acid tolerance has been
390 previously demonstrated in other bacteria. By being able to control both total abundance
391 and the stoichiometry of different hopanoid species, we showed that only the former
392 dictated survival at low pH. This finding suggests distinct mechanisms by which these two
393 chemical stresses influence membranes, and therefore how this class of lipids can protect
394 against them. Specifically, low pH does not disrupt the integrity of *Z. mobilis* membranes
395 (Fig. 5D) while ethanol, as a solvent stress, does has such a structural effect.
396

397 Using a spectroscopic probe for membrane structure (Laurdan), we characterized the
398 interplay of increasing ethanol concentrations and hopanoid composition on membrane
399 structure. These experiments showed that *Z. mobilis*-derived membranes undergo
400 ethanol-mediated structural changes previously identified in model bilayers. Hopanoids
401 alter the magnitude of these effects and the ethanol concentrations at which they take
402 place. Although the parameters for phase transitions in extracted membranes might not
403 exactly correspond to those in intact cells, it is worth considering their physiological
404 relevance. The toxicity threshold for ethanol in cells – around 20% v/v – corresponds to
405 an interdigitated state we observed in liposomes. Although membranes are ordered in
406 this state, they are also highly leaky (Zeng, Smith, & Chong, 1993), consistent with
407 SYTOX staining of cells in 20% ethanol. Accordingly, the mutant with reduced hopanoid
408 amount (*hpnC*) showed the strongest interdigitated effect, as measured by increase in
409 Laurdan GP, and also the lowest survival under acute ethanol toxicity. Evaluating how
410 hopanoids modulate ethanol-membrane interactions *in vitro* thus provides a mechanism
411 by which they could act to increase physiological tolerance *in vivo*.
412
413 Hopanoids are commonly thought to mimic the effects of eukaryotic sterols, whose planar
414 structures condense lipid bilayers, reducing the area per phospholipid, and acyl chain
415 mobility (Yeagle, 1985). These effects on membrane ordering (Fig. 3) lower the
416 permeability of polar molecules across the bilayer, including protons (Deamer & Nichols,
417 1989). A reduction in proton leakage into the cytoplasm provided by the presence of
418 abundance hopanoids or sterols provides a straightforward mechanism for acid tolerance
419 imparted by these lipids. During ethanol stress, hopanoids instead act to mediate the
420 phase properties of membranes: bilayer expansion at low concentrations, interdigitation
421 at medium concentrations, and dissolution at higher concentrations. All these transitions
422 are likely resisted by the increased packing of lipids that triterpenoids impart. Notably,
423 cholesterol has previously been shown to resist the interdigitated phase transition in lipid
424 vesicles (Tierney, Block, & Longo, 2005). In this way the interplay of hopanoids and
425 ethanol mimics that of sterols or other triterpenoids.
426

427 One way hopanoids differ from other triterpenoids is in their polar head groups, which
428 feature elongated polyhydroxylated moieties. Elongated hopanoids make up ~90% of all
429 species in *Z. mobilis* and we found that their composition also mediates ethanol tolerance.
430 We propose a very different functional analogue for these structures: di-acyl glycerol lipids
431 modified by one or more sugar groups (glycolipids), which are highly abundant in plant
432 thylakoid and in cell-wall less bacteria. Glycolipids promote membrane ordering through
433 hydrogen bonding interactions between adjacent lipid head groups (Curatolo, 1987). The
434 phase behavior of glycolipid-containing membranes can be mediated by changes in head
435 group structure, such as the type of glucoside linkage in a disaccharide (Iwamoto,
436 Sunamoto, Inoue, Endo, & Nojima, 1982). Sugar-modified lipids, including glycolipids,
437 hopanoids, and ceramides, could act as a general mechanism to buffer membrane
438 structure against chemical agents (solvents, detergents) or other physical stresses
439 (temperature, shear forces) that alter hydrophobic interactions. Hopanoids, however, are
440 unique in that they feature both hydrocarbon and polar structural elements that promote
441 bilayer stability. It is likely that the combination of these features allows different
442 hopanoids species to maintain membrane stability in response to the wide-range of
443 environmental challenges experienced by bacterial cells.
444
445
446 **Experimental Procedures:**
447
448 *Cell growth and physiology: Z. mobilis* strains were grown in rich medium (RM) (10 g/L
449 yeast extract (Becton Dickinson), 2 g/L potassium phosphate dibasic, and 20 g/L glucose,
450 pH 6.2) in culture tubes shaking at 200 rpm at 30°C, unless otherwise noted. For mutants,
451 the medium was supplemented with kanamycin (100 µg/mL). For each culture, 5 mL of
452 medium was inoculated from a glycerol stock and strain was allowed to grow for 2 to 3
453 days under selection. Cultures were then back-diluted into 10 mL fresh medium; the
454 inoculation ratio was varied across ZM4 mutants (from 0.1% to 2.5% v/v) to account for
455 growth rate variability and enable harvesting after 20-22 hours in early stationary phase.
456 Cells were then harvested for lipid, DNA extraction, or toxicity tests. For lipid analysis,

457 characteristic cultures of each mutant were also dried to completeness and massed, in
458 order to correlate optical density to cell dry mass.
459
460 For *E. coli* experiments, K12 cells (MG1655) were grown in MOPS minimal medium pH
461 7.2 (Teknova) with 0.6% (w/v) succinic acid as the carbon source. Cells were grown to
462 early stationary phase (OD ~ 1.0) at 30°C in 10 mL cultures before being harvested for
463 ploidy quantification and to stationary phase (OD ~ 2.0) in 50 mL Luria Broth medium for
464 lipid extractions.
465
466 For fitness analysis, *Z. mobilis* growth curves were recorded in 1 mL cultures in 24-well
467 plates (Falcon) inoculated with 10 µL of overnight culture. The plates were sealed with a
468 semi-permeable film (Thermo Fischer) and incubated at 30°C in a Synergy 4 plate reader
469 (BioTek) with shaking and absorbance readings (600 nm) every five minutes, for 24 to 72
470 hours. For acute toxicity measurements, cells were spun down in early stationary phase
471 and resuspended in RM (control) and RM supplemented with ethanol (20% v/v) or HCl
472 (until pH 2.5). After incubation (30 min), cells were serially diluted and plated on RM agar
473 plates in technical triplicates. Cell survival was measured by the ratio of colony forming
474 units (CFUs) compared to the control condition. For assaying of permeabilization, cells
475 were incubated with 30 nM of SYTOX Green Dead Cell Stain (Invitrogen) for 15 minutes.
476 The fluorescence intensity of 100,000 cells was then measured on an Accuri flow
477 cytometer (BD) using a GFP fluorescence filter set. Data was analyzed and plotted using
478 FlowJo.
479
480 *Genetic analyses:* The function of each *hpn* gene was deduced from their roles described
481 by loss of function studies in other bacteria (Bradley, Pearson, Saenz, & Marx, 2010;
482 Schmerk et al., 2015; Welander et al., 2012). For PCR and copy number measurements,
483 2 mL of cultures grown to early stationary phase and genomic DNA extracted with a
484 Wizard Genomic DNA Purification Kit (Promega). Outside-in colony PCR of a subset of
485 *hpn* genes was performed with PrimeSTAR DNA polymerase (TaKaRa) using the
486 following primers:
487

488 *hpnC*: CCACATGATTTCCCGTTCAGCTTATG and CCGGTTCTTTCAGAAAAGCGGC
489 *hpnI*: GCCAAGGGCTTCGAGTTACTATAAACT and TGACTTTTTTAAGAGCCGCTACGGT
490 *hpnJ*: CGGAAGTGCGGTCACTTATCCC and ACTGAGAAGCCCTTAGAGCC
491
492 For quantifying transposon insertion rates, genomic DNA libraries were prepared using
493 NEBnext DNA Library Prep Master Mix Set for Illumina (New England Biolabs) following
494 the instructions for 400 bp insert libraries. Sequencing was performed using the 600-cycle
495 Miseq Reagent Kit v3 (Illumina) on the MiSeq system (Illumina). For analysis, the online
496 platform Galaxy (usegalaxy.org) was used, with alignments performed with the *Map with*
497 *BWA-MEM* tool to ZM4 genomes to which a typical transposon sequence (KanR Tn5 with
498 an inserted TagModule) had been juxtaposed. The resulting alignment file was opened
499 with UGENE and the fragments aligned to the border of the transposon were examined
500 to find the transposon insertion locus. The genome files were updated with actual
501 transposon insertions and the alignment was repeated. The coverage depth was
502 calculated with *plotCoverage* tool. To estimate the transposon insertion rate, the mean
503 coverage depth over the whole genome was computed and compared to the mean
504 coverage depth of a 500 bp conserved region inside the transposon's KanR cassette.
505
506 Quantification of ploidy was performed using qPCR as previously described (Pecoraro,
507 Zerulla, Lange, & Soppa, 2011). Briefly, cells were harvested at early stationary phase
508 and serially diluted. A hemocytometer was used to count the density of cells in the
509 dilutions, and solutions containing discrete number of cells were then prepared. From
510 these, genomic DNA was quantitatively extracted using phenol:chloroform extraction after
511 cell lysis, as previously described (Thompson et al., 2018). Separately, standards
512 containing the two targeted loci were amplified from *Z. mobilis* (Z1, Z2) and *E. coli*
513 genomic DNA (E1, E2) using the following primers:
514
515 Z1 standard: TTGTGTTAAAGGGAGCGAGAC and AGACATATGTCCACGGACTTCTAA
516 Z2 standard: AATTTCAAAGGGGCCTTAGCT and TTAAAGACCCTCCTACTGCTTGT
517 E1 standard: ATTGCCCATAAACGAGAATACC and GGAAGCTTGGATCAACCG
518 E2 standard: TAACGCGTCGTCTGAAACC and TAGACGCCAGCATGTTCGTAA

519

520 The single-product amplification of the resulting standards, 1 KB in length, was confirmed
521 by agarose electrophoresis, which was then purified by a PCR cleanup kit (Qiagen). The
522 concentration of the standard was quantified by absorbance at 260 nm and then serially
523 diluted to prepare a standard curve. PCR reactions for both gDNA samples and the
524 standards was prepared with SYBR Green Master Mix (Invitrogen), using primer pairs
525 that amplified a ~250-bp insert in the standards above:

526

527 Z1 analysis: `TAAACAGCCTTTAAAATTTTGTGTTCTTG` and
528 `GTTTATTTTCGGTATTTTTGACGCAG`
529 Z2 analysis: `ATTTCGATATTGTTCTGCAGTATCG` and
530 `TACTCAAGACCTTCAATATTGTTTTAACAT`
531 E1 analysis: `AAACTGGATACCCGCCTG` and `CCTTTTGACGTCATCATCATTG`
532 E2 analysis: `ATCCGTGATGAAGTGGGG` and `AATGCAGTAACCACAGCC`

533

534 Amplification was measured on a StepOnePlus Real-Time PCR System (Applied
535 Biosystems). Quantification of gDNA abundance relative to the standard curve was
536 performed using the ΔC_T method.

537

538 *Lipid analyses:* The lipid extraction protocol used in this study was adapted from Bligh
539 and Dyer (Bligh & Dyer, 1959). Cell pellets from 10 mL of culture were resuspended in a
540 400 microliters of water and sonicated for 10 minutes at 50°C. Chloroform and methanol
541 (1:1, 5 mL) were added and the monophasic extraction mixture was bath sonicated for 1
542 hour at 50°C and then left to shake for 3 hours at 37°C. Water (2.5 mL) was then added
543 and complete separation of the organic (chloroform) and water/methanol phases was
544 achieved through centrifugation. The organic phase was collected and evaporated to
545 dryness under N_2 flux.

546

547 For analysis of hopene and diplopterol by GC-MS, dry lipids were silylated in 150 µL of
548 N,O-Bis (trimethylsilyl) trifluoroacetamide (BSTFA kit, Supelco) and 150 µL of pyridine for
549 2 hours at 50°C. The solvent was then evaporated under N_2 flux. The product was then

550 extracted in hexane (100 µL) and filtered (Nylon 0.2 µm 500 µL centrifugal filters, VWR)
551 before analysis. Gas chromatography was performed on an HP 6890 Series GC-System
552 (Hewlett Packard) equipped with a DB-5MS capillary column (30 m length x 0.25 mm
553 internal diameter, 25 µm film; J&W). 1 µL of sample was injected at a temperature of
554 250°C and the GC was run in splitless mode with a Helium (carrier gas) flow rate of
555 1 mL/min at a pressure of 9.36 psi. The temperature program of the oven was as follows:
556 held at 80°C for 1 min after injection, heated to 280°C at 20°C/min, held at 280°C for
557 15 min, heated to 300°C at 20°C/min and held for 7 min. The column was coupled to a
558 HP 5973 Mass Selective Detector (Hewlett Packard). The source and quad temperature
559 were set to 300°C and 200°C, respectively. The solvent delay was set to 9 min. For
560 quantification of C_{30} hopanoids, the SIM mode (191 *m/z* for hopene and 131 *m/z* for
561 diplopterol) was used with a dwell time of 100 ms and 3 cycles/s. Data collection and
562 processing were performed with HP Enhanced ChemStation software (Agilent
563 Technologies).
564
565 For analysis of elongated hopanoids, lipid extraction was performed as described above,
566 with a known amount (100 µg) of an internal standard (5α-pregnane-3β,20β-diol) added
567 to the extraction mixture. The following derivatization procedure was adapted from Talbot
568 et *al.* (Talbot, Summons, Jahnke, & Farrimond, 2003) The dried chloroform extract was
569 acetylated in 3 mL of acetic anhydride/pyridine (1:1 v/v) at 50°C for 1 hour and left stand
570 overnight at room temperature. The solvent was then evaporated under N_2 flux and the
571 acetylated lipids were dissolved in 250 µL of methanol/isopropanol (6:4 v/v). The samples
572 were centrifuged for 10 minutes at maximum speed and transferred to glass vials. Liquid
573 chromatography was performed with a Kinetex XB-C18 column (100 mm length x 2.1 mm
574 internal diameter, 2.6 µm particle size; Phenomenex) at 50°C, with a 1200 Series HPLC
575 system (Agilent Technologies). The injection volume was 3 µL and separation was
576 achieved with a flow-rate of 0.45 mL/min and the following mobile phase gradient profile:
577 20% to 42% B in 2.2 min, held at 42% B for 3.6 min, 42% to 100% B in 0.1 min, held at
578 100% B for 2.1 min, 100% to 20% B in 0.1 min, held at 20% B for 4.3 min (where solvent
579 A is composed of 30% isopropanol/40% methanol/30% water, and solvent B of 90%
580 isopropanol/10% water; HPLC grade, Honeywell Burdick & Jackson). The HPLC system

581 was coupled to an Agilent Technologies 6210 time-of-flight mass spectrometer (LC-TOF
582 MS), with 1/5 post-column split, via a LAN card. Nitrogen was used as nebulizing (6 L/min)
583 and drying (300°C, 30 lb/in^2) gases. The vaporizer temperature was 250°C. The corona
584 was set to 7 μA. Atmospheric pressure chemical ionization (APCI) was conducted in the
585 positive ion mode with a capillary voltage of 3000 V. Full-scan mode (100–1500 *m/z*) at
586 1 spectrum/s was used for MS experiments. TOF-MS was calibrated with Agilent APCI
587 TOF tuning mix. Data acquisition and integration were performed by the MassHunter
588 Workstation (Agilent Technologies) and MassHunter Qualitative Analysis (Agilent
589 Technologies), respectively. The targeted ions are presented in Table S2; quantified
590 analytes were normalized to the internal standard in order to correct for variations in
591 ionization strength.
592
593 *Biophysical analyses:* Liposomes were prepared from lipids extracted from early
594 stationary phase cells (100 mL) using a scaled-up version of the procedure described
595 above. Upon complete drying of the organic phase under vacuum, the extracted lipids
596 were massed and solubilized in chloroform at 1 mg/mL. For each liposome preparation,
597 300 μL of the lipid solution was transferred to a borosilicate test tube and dried with Argon.
598 The resulting film was further dried for 1 hour under vacuum. Liposomes were formed by
599 resuspending the film in buffer (20 mM HEPES, pH 7.0), followed by overnight incubation
600 with gentle agitation. Liposome formation was confirmed by microscopy of the samples
601 labeled with Rhodamine 6G, a membrane dye. Before analysis, liposomes were extruded
602 to 100 nm with a miniextruder (Avanti Polar Lipids).
603
604 For DPH experiments, liposomes were incubated with 0.5% (v/v) of a 5 mM DPH (Sigma)
605 stock solution in ethanol. Samples were then incubated for at least one hour under gentle
606 agitation. Steady-state anisotropy was measured using a Fluorolog spectrofluorometer
607 (Horiba) with automated polarizers; excitation was set to 360 nm, and emission at 430
608 nm. For Laurdan experiments, liposomes were incubated with 1.0% (v/v) of a 1 mg/ml
609 stock solution of Laurdan (Invitrogen) in DMSO. Laurdan emission was measured from
610 380 to 600 nm upon excitation at 365 nm. Laurdan GP was calculated as the ratio of

integrated emission intensities at two different ranges of wavelengths: GP = ($I_{420\text{-}440nm}$ – $I_{490\text{-}510nm}$) / ($I_{420\text{-}440nm}$ + $I_{490\text{-}510nm}$).

Acknowledgments: Dr. Jeffrey Skerker kindly provided strains and technical assistance. Tristan de Rond, Patrick Shih, Mitchell Thompson, and Meytal Higgins provided helpful discussions. This work was part of the DOE Joint BioEnergy Institute (http://www.jbei.org) supported by the U. S. Department of Energy, Office of Science, Office of Biological and Environmental Research, through contract DE-AC02-05CH11231 between Lawrence Berkeley National Laboratory and the U. S. Department of Energy. This work was also supported by National Science Foundation grants MCB-1442724 and MCB-1715681 to J.D.K. The authors declare no conflicts of interest.

Author contributions: L.B., J.K.D., and I.B. conceived the study and designed the experiments. L.B. and E.E.K.B. performed lipid analysis. L.B. and I.B. performed all other experiments. All authors discussed the results and wrote the paper.

Graphical abstract:

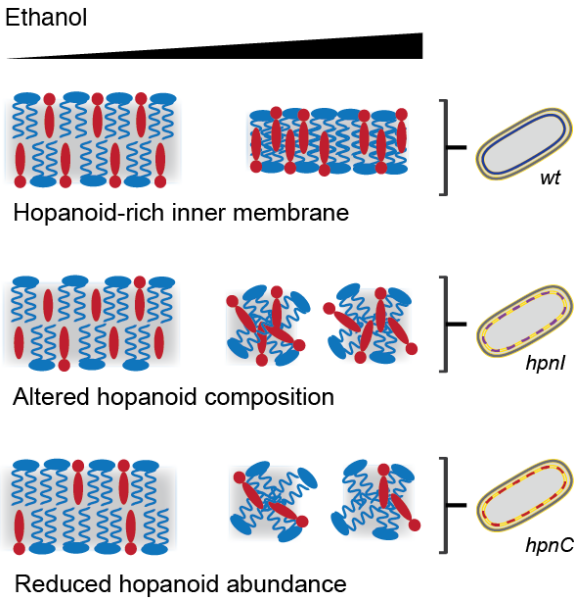

Abbreviated Summary: A set of knockdown, transposon mutants was used to analyze the physiological functions of hopanoid composition in the ethanologenic bacterium *Zymomonas mobilis*. Both the abundance of hopanoids and their stoichiometry mediated growth and survival in ethanol-rich medium. Liposome-based experiments showed that hopanoids mediate the concentrations at which ethanol-induced transitions in membrane structure occur, providing a mechanism for their protective effects.

References:

Bligh, E. G., & Dyer, W. S. (1959). A rapid method of total lipid extraction and purification. *Canadian Journal of Biochemistry and Physiology*, *37*, 911–917.

Bradley, A. S., Pearson, A., Saenz, J. P., & Marx, C. J. (2010). Adenosylhopane: The first intermediate in hopanoid side chain biosynthesis. *Organic Geochemistry*, *41*(10), 1075–1081.

Bringer, S., Thomas, H., Poralla, K., & Sahm, H. (1985). Influence of ethanol on the hopanoid content and the fatty acid pattern and continuous cultures of Zymomonas mobilis. *Archives of Microbiology*, *2*, 312–316.

Curatolo, W. (1987). The physical properties of glycolipids. *Biochimica et Biophysica Acta*, *906*, 111–136.

Deamer, D. W., & Nichols, J. W. (1989). Proton flux mechanisms in model and biological membranes. *The Journal of Membrane Biology*, *107*(2), 91–103.

Espenshade, P. J., & Hughes, A. L. (2007). Regulation of Sterol Synthesis in Eukaryotes. *Annual Review of Genetics*, *41*(1), 401–427.

Flamholz, A., Noor, E., Bar-Even, A., Liebermeister, W., & Milo, R. (2013). Glycolytic strategy as a tradeoff between energy yield and protein cost. *Proceedings of the National Academy of Sciences of the United States of America*, *110*(24), 10039–44.

Gurtovenko, A. A., & Anwar, J. (2009). Interaction of ethanol with biological membranes: The formation of non-bilayer structures within the membrane interior and their significance. *Journal of Physical Chemistry B*, *113*(7), 1983–1992.

He, M., Wu, B., Qin, H., Ruan, Z., Tan, F., Wang, J., … Hu, Q. (2014). Zymomonas mobilis: a novel platform for future biorefineries. *Biotechnology for Biofuels*, *7*(1), 101.

He, M., Wu, B., Shui, Z., Hu, Q., Wang, W., Tan, F., … Su, X. (2012). Transcriptome profiling of Zymomonas mobilis under ethanol stress. *Biotechnology for Biofuels*, *5*(1), 75.

Hermans, M. A. F., Neuss, B., & Sahm, H. (1991). Content and Composition of Hopanoids in Zymomonas mobilis under Various Growth Conditions. *Journal of Bacteriology*, *173*(17), 5592–5595.

Holte, L. L., & Gawrisch, K. (1997). Determining ethanol distribution in phospholipid multilayers with MAS- NOESY spectra. *Biochemistry*, *36*(15), 4669–4674.

Iwamoto, K., Sunamoto, J., Inoue, K., Endo, T., & Nojima, S. (1982). Importance of surface structure in liposomal membranes of glyceroglycolipids. *Biochimica et Biophysica Acta*, *691*, 44–51.

Kannenberg, E., Blume, A., McElhaney, R., & Poralla, K. (1983). Monolayer and calorimetric studies of phosphatidylcholines containing branched-chain fatty acids and of their interactons with cholesterol and with a bacterial hopanoid in model membranes. *Biochimica et Biophysica Acta*, *733*, 111–116.

Kulkarni, G., Busset, N., Molinaro, A., Gargani, D., Chaintreuil, C., Silipo, A., … Newman, D. K. (2015). Specific hopanoid classes differentially affect free-living and symbiotic states of bradyrhizobium diazoefficiens. *MBio*, *6*(5), 1–9.

Lee, K. J., Skotnicki, M. L., Tribe, D. E., & Rogers, P. L. (1980). Kinetic Studies on a Highly Productive Strain of Zymomonas Mobilis. *Biotechnology Letters*, *2*(8), 339–344.

Moreau, R. A., Powell, M. J., Fett, W. F., & Whitaker, B. D. (1997). The effect of ethanol and oxygen on the growth of Zymomonas mobilis and the levels of hopanoids and other membrane lipids. *Current Microbiology*.

Mou, J., Yang, J., Shao, Z., & Huang, C. (1994). Alcohol Induces Interdigitated Domains in Unilamellar Phosphatidylcholine Bilayers. *Biochemistry*, *33*(33), 9981–9985.

Ourisson, G., & Rohmer, M. (1992). Biohopanoids: A Novel Class of Bacterial Lipids. *Accounts of Chemical Research*, *25*(9), 403–408.

Parasassi, T., Krasnowska, E. K., Bagatolli, L., & Gratton, E. (1998). Laurdan and Prodan as polarity-sensitive fluorescent membrane probes. *J Fluorescence*, *8*(4), 365–373.

Pearson, A., Budin, M., & Brocks, J. J. (2003). Phylogenetic and biochemical evidence for sterol synthesis in the bacterium Gemmata obscuriglobus. *Proc Natl Acad Sci U S A*, *100*(26), 15352–15357.

Pearson, A., Flood Page, S. R., Jorgenson, T. L., Fischer, W. W., & Higgins, M. B. (2007). Novel hopanoid cyclases from the environment. *Environmental Microbiology*, *9*(9), 2175–2188.

Pecoraro, V., Zerulla, K., Lange, C., & Soppa, J. (2011). Quantification of ploidy in proteobacteria revealed the existence of monoploid, (mero-)oligoploid and polyploid species. *PLoS ONE*, *6*(1).

Perzl, M., Reipen, I. G., Schmitz, S., Poralla, K., Sahm, H., Sprenger, G. A., & Kannenberg, E. L. (1998). Cloning of conserved genes from Zymomonas mobilis and Bradyrhizobium japonicum that function in the biosynthesis of hopanoid lipids. *Biochimica et Biophysica Acta - Lipids and Lipid Metabolism*, *1393*(1), 108–118.

Poger, D., & Mark, A. E. (2013). The relative effect of sterols and hopanoids on lipid bilayers: When comparable is not identical. *Journal of Physical Chemistry B*, *117*(50), 16129–16140.

Rohmer, M., Bouvier-Nave, P., & Ourisson, G. (1984). Distribution of hopanoid triterpenes in prokaryotes. *Microbiology*, *130*(5), 1137–1150.

Saenz, J. P., Sezgin, E., Schwille, P., & Simons, K. (2012). Functional convergence of hopanoids and sterols in membrane ordering. *Proceedings of the National Academy of Sciences*, *109*(35), 14236–14240.

Schmerk, C. L., Bernards, M. A., & Valvano, M. A. (2011). Hopanoid production is required for low-pH tolerance, antimicrobial resistance, and motility in Burkholderia cenocepacia. *Journal of Bacteriology*, *193*(23), 6712–6723.

Schmerk, C. L., Welander, P. V., Hamad, M. A., Bain, K. L., Bernards, M. A., Summons, R. E., & Valvano, M. A. (2015). Elucidation of the Burkholderia cenocepacia

722 hopanoid biosynthesis pathway uncovers functions for conserved proteins in
723 hopanoid-producing bacteria. *Environmental Microbiology*, *17*(3), 735–750.
724 Simon, S. A., & McIntosh, T. J. (1984). Interdigitated hydrocarbon chain packing causes
725 the biphasic transition behavior in lipid/alcohol suspensions. *BBA - Biomembranes*,
726 *773*(1), 169–172.
727 Skerker, J. M., Leon, D., Price, M. N., Mar, J. S., Tarjan, D. R., Wetmore, K. M., …
728 Arkin, A. P. (2013). Dissecting a complex chemical stress: chemogenomic profiling
729 of plant hydrolysates. *Molecular Systems Biology*, *9*(674), 21.
730 Sprenger, G. A. (1996). Carbohydrate Metabolism in Zymomonas mobilis: a Catabolic
731 Highway With Some Scenic Routes, *145*, 301–307.
732 Suurkuusk, J., Lentz, B. R., Barenholz, Y., Biltonen, R. L., & Thompson, T. E. (1976). A
733 Calorimetric and Fluorescent Probe Study of the Gel-Liquid Crystalline Phase
734 Transition in Small, Single-Lamellar Dipalmitoylphosphatidylcholine Vesicles.
735 *Biochemistry*, *15*(7), 1393–1401.
736 Swings, J., & De Ley, J. (1977). The biology of Zymomonas. *Bacteriological Reviews*,
737 *41*(1), 1–46.
738 Talbot, H. M., Summons, R., Jahnke, L., & Farrimond, P. (2003). Characteristic
739 fragmentation of bacteriohopanepolyols during atmospheric pressure chemical
740 ionisation liquid chromatography/ion trap mass spectrometry. *Rapid*
741 *Communications in Mass Spectrometry*, *17*(24), 2788–2796.
742 Thomas, D. S., Hossack, J. A., & Rose, A. H. (1978). Plasma-membrane lipid
743 composition and etehanol tolerance in Saccharomyces cerevisiae. *Archives of*
744 *Microbiology*, *117*, 239–245.
745 Thompson, M. G., Sedaghatian, N., Barajas, J. F., Wehrs, M., Bailey, C. B., Kaplan, N.,
746 … Keasling, J. D. (2018). Isolation and characterization of novel mutations in the
747 pSC101 origin that increase copy number. *Scientific Reports*, *8*(1), 1–11.
748 Tierney, K. J., Block, D. E., & Longo, M. L. (2005). Elasticity and phase behavior of
749 DPPC membrane modulated by cholesterol, ergosterol, and ethanol. *Biophysical*
750 *Journal*, *89*(4), 2481–2493.
751 Vierl, U., Löbbecke, L., Nagel, N., & Cevc, G. (1994). Solute effects on the colloidal and
752 phase behavior of lipid bilayer membranes: ethanol-dipalmitoylphosphatidylcholine
753 mixtures. *Biophysical Journal*, *67*(3), 1067–1079.
754 Welander, P. V., Doughty, D. M., Wu, C. H., Mehay, S., Summons, R. E., & Newman,
755 D. K. (2012). Identification and characterization of Rhodopseudomonas palustris
756 TIE-1 hopanoid biosynthesis mutants. *Geobiology*, *10*(2), 163–177.
757 Welander, P. V., Hunter, R. C., Zhang, L., Sessions, A. L., Summons, R. E., & Newman,
758 D. K. (2009). Hopanoids play a role in membrane integrity and pH homeostasis in
759 Rhodopseudomonas palustris TIE-1. *Journal of Bacteriology*, *191*(19), 6145–6156.
760 Yeagle, P. L. (1985). Cholesterol and the cell membrane. *BBA - Reviews on*
761 *Biomembranes*, *822*(3–4), 267–287.
762 You, K. M., Rosenfield, C., & Knipple, D. C. (2003). Ethanol tolerance in the yeast
763 Saccharomyces cerevisiae is dependent on cellular oleic acid content. *Applied and*
764 *Environmental Microbiology*, *69*(3), 1499.
765 Zeng, J., & Chong, P. L. (1995). Effect of ethanol-induced lipid interdigitation on the
766 membrane solubility of Prodan, Acdan, and Laurdan. *Biophysical Journal*, *68*(2),
767 567–573.

Zeng, J., Smith, K. E., & Chong, P. L. (1993). Effects of alcohol-induced lipid interdigitation on proton permeability in L-alpha-dipalmitoylphosphatidylcholine vesicles. *Biophysical Journal*, *65*(4), 1404–1414.

Supporting Information

Distinct functional roles for hopanoid composition in the chemical tolerance of *Zymomonas mobilis*

Léa Brenac, Edward E.K. Baidoo, Jay D. Keasling, and Itay Budin

This file contains Tables S1-S2 and Figures S1-S4.

785 **Table S1:** *Z. mobilis* ZM4 mutants used in this study. Insertion sites provide the genome
786 location of the repeat region, the sequence immediately before the transposon insertion;
787 the same sequence is repeated at the end of the transposon. Tn5 frequency is the fraction
788 of alleles containing the transposon, as measured by deep sequencing.
789

Gene code	Gene symbol	Gene product	Insertion site (bp)	Direction of Tn5	Tn5 frequency (%)
hpnC	ZMO0869	squalene synthase	878429-878437	forward	31
hpnD	ZMO0870	squalene synthase	878952-878960	reverse	35
hpnF	ZMO0872	squalene hopene cyclase	882157-882165	reverse	99
shc	ZMO1548	squalene hopene cyclase	1579153-1579161	reverse	100
hpnG	ZMO0873	phosphorylase	883206-883214	forward	43
hpnH	ZMO0874	radical SAM protein	884303-884311	reverse	25
hpnI	ZMO0972	glycosylase	987434-987442	forward	59
hpnJ	ZMO0973	radical SAM protein	989161-989169	forward	98
hpnK	ZMO0974	polysaccharide hydrolyase	990783-990791	reverse	92
Control	ZMO0047	lysine exporter protein	45590-45598	forward	100

790
791
792 **Table S2:** Base peaks of targeted analytes for LC-APCI-TOF-MS analysis of elongated
793 hopanoids used in this study. Designated acetylated structures for the compounds are
794 shown in Fig. S2c.
795

Compound	Acetylated structure	Base peak	Corresponding ion
BHT	I	655.50 *m/z*	$[M+H-CH_3COOH]^+$
BHT ether	II	1002.62 *m/z*	$[M+H]^+$
BHT glucosamine	III	1002.62 *m/z*	$[M+H]^+$
5α-pregnane-3β,20β-diol (standard)	IV	345.28 *m/z*	$[M+H-CH_3COOH]^+$

796
797
798

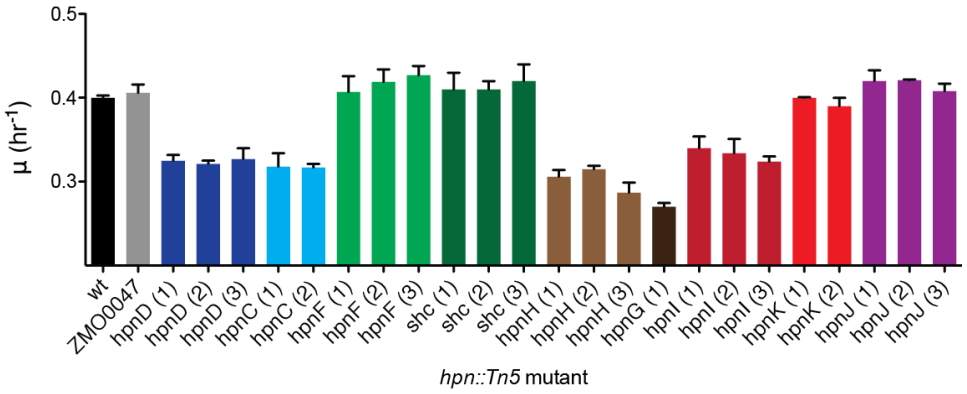

Fig. S1: Redundant mutants of *hpn* genes, which feature Tn5 insertions in different sites, feature identical exponential growth rates (μ), indicating that all act similarly as loss of function mutations. Wild type cells (wt) and a kanamycin resistant control (ZMO0047, with a Tn5 insertion in a non-essential lysine exporter) are used as controls throughout this study. Because each redundant mutant featured similar fitness (e.g. *hpnD* (1) vs. *hpnD* (2)) only one of them was chosen for further genetic, chemical, and physiological analysis. Colors indicate mutants of the same gene. Error bars indicate SD.

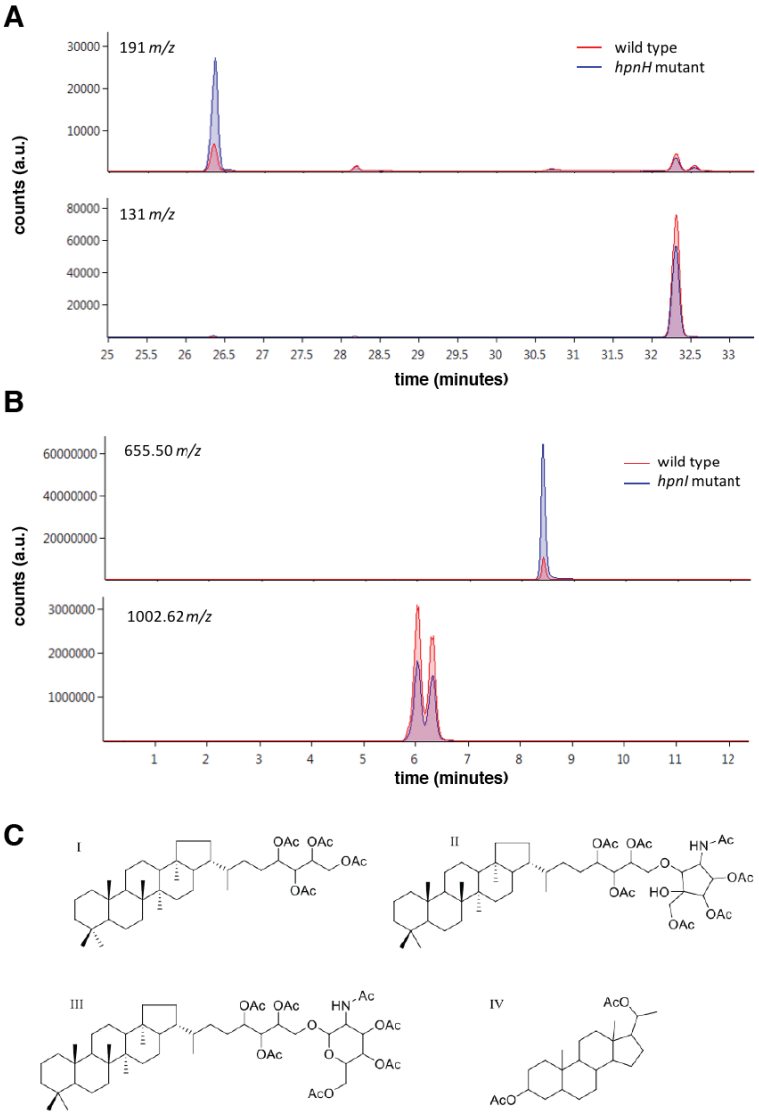

Fig. S2: Sample chromatograms for hopanoid analyses methods used in this study. (**A**) GC-MS chromatograms showing the characteristic fragments for hopene (191 *m/z*, top) and diplopterol (131 *m/z*, bottom) for silylated lipids from a wild type *Z. mobilis* culture and one carrying a Tn5 insertion in *hpnH*. Because HpnH utilizes hopene as a substrate, the *hpnH* mutant features increased hopene, but not diploterol, levels. (**B**) APCI-LC-TOF-MS chromatograms showing the characteristic ions for acetylated lipids from a from a wild type *Z. mobilis* culture and one carrying a Tn5 insertion in *hpnI*. The mutant features reduced amounts of BHT (655.50 *m/z* representing $[M+H-CH_3COOH]^+$ for BHT, top) but reduced amounts of BHT glucosamine and BHT cyclitol ether (1002.62 *m/z* representing $[M+H]^+$ for both species, bottom). The latter species are isomers, so they feature identical

821 masses but can be separated by liquid chromatography. HpnI utilizes BHT as a substrate,
822 so the accumulation of BHT is consistent with reduced copy numbers of *hpnI*. (**c**)
823 Structure compounds analyzed by LC-APCI-TOF-MS; I-III represent acetylated hopanoid
824 species, while IV is an acetylated internal standard.
825

826
827

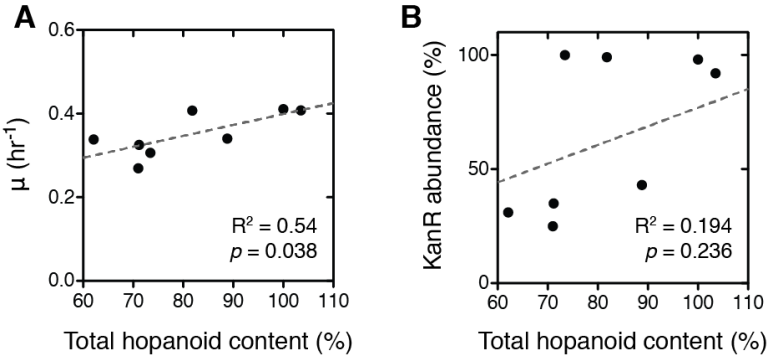

828
829
830 **Fig. S3:** Growth rates (μ) of *hpn* mutants are significantly correlated with total hopanoid
831 content (**A**) but not to the frequency of Tn5 alleles, as measured by sequencing read
832 depth (**B**). Hopanoid content is presented as a % relative to wild type cells. *P*-values
833 represent significance tests assessing if the slope of the linear regression is non-zero.
834

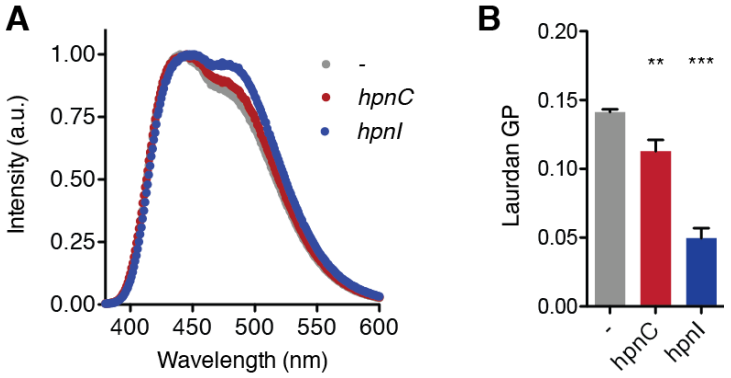

Fig. S4: The emission spectra for Laurdan (excitation at 364 nm) incubated in liposomes assembled from extracted *Z. mobilis* lipids. Liposomes from control cells (-), featuring intact hopanoid compositions, exhibit a Laurdan emission spectrum that is blue shifted compared to those from cells with reduced (*hpnC*) or altered (*hpnI*) hopanoid levels. This emission difference, quantified by General Polarization (GP) values in the text, measures solvation of the membrane. Increased presence of polar solvent leads to relaxation of the excited dye, thereby red-shifting its emission in membranes that are less ordered near the head group-hydrocarbon interface. Error bars indicate mean +/- SD, n = 3 independent liposome preparations. Unpaired t-tests were used to assess significance against liposomes with intact hopanoids: **, $p < 0.01$; ***, $p < 0.001$.